Chapter-4

A Molecular Theory of the Effect of a Strong Electric Field on Phase Transitions in Highly Polar Compounds

4.1 Introduction

As we have described earlier, many mesogenic compounds exhibit both nematic (N) and smectic A (SmA) phases. The N phase has a long range orientational order of the long axes of rod like molecules [1]. The SmA phase has an additional translational order of the centres of mass along the director $\hat{\boldsymbol{n}}$, which is a unit vector representing the average orientation direction of the molecules. Liquid crystals composed of highly polar compounds exhibit double re-entrance and other unusual phase transitions [1]. In the pervious chapters, we have developed a molecular theory to describe these phase transitions. In this chapter, we extend the model to include the effect of an external electric field on some of these phase transitions and calculate the electric field-temperature phase diagrams.

An important property of a uniaxial liquid crystalline medium is the dielectric anisotropy. It is defined as the difference between the dielectric constants[†] measured with the electric field applied parallel and perpendicular to the director ($\hat{\boldsymbol{n}}$), *i.e.,*

$$\Delta\varepsilon = \varepsilon_{\parallel} - \varepsilon_{\perp}. \tag{4.1}$$

When an electric field is applied to a nematic liquid crystal, the field couples to the director through the dielectric anisotropy and tends to align the molecules parallel or perpendicular to the field depending on the sign of the anisotropy.

The field dependent free energy density is given by,

$$F^{\mathrm{E}} = -\frac{1}{2}\,\varepsilon_0\,\varepsilon_{\parallel}\mathcal{E}^2\cos^2\theta - \frac{1}{2}\,\varepsilon_0\,\varepsilon_{\perp}\mathcal{E}^2\sin^2\theta \tag{4.2}$$

where $\mathcal{E}$ is the magnitude of the electric field, ε_0 is the absolute permittivity of vacuum and θ is the angle made by the director with the direction of the applied field. In terms of $\Delta\varepsilon$, equation 4.2 can be written as,

$$F^{E} = -\frac{1}{2}\,\varepsilon_0\,\Delta\varepsilon\,(\hat{\boldsymbol{n}}\cdot\vec{\mathcal{E}})^2 - \frac{1}{2}\,\varepsilon_0\varepsilon_\perp\mathcal{E}^2. \tag{4.3}$$

When the electric field is low, $\varepsilon_\parallel$ and $\varepsilon_\perp$ remain practically unchanged. Thus, to minimise the free energy density, the director aligns parallel to the field for a nematic with positive $\Delta\varepsilon$ and perpendicular to the field when $\Delta\varepsilon$ is negative.

Usually, a medium with nonpolar rod like molecules will have a small positive $\Delta\varepsilon$ (<1) due to the anisotropy in the polarisability of the molecules. However, when the molecule has one or more permanent dipoles, the orientational contribution to the dielectric constant becomes important. For nematic liquid crystals consisting of polar molecules with dipoles *along* the long axes, $\Delta\varepsilon$ can be as large as +20 or higher. We restrict our discussion to materials with positive $\Delta\varepsilon$. When the electric field is applied parallel to the director, from equation 4.2, we obtain

$$F^{E} = -\frac{1}{2}\,\varepsilon_0\,\varepsilon_\parallel\mathcal{E}^2. \tag{4.4}$$

When the applied field is strong, $\varepsilon_\parallel$ can increase to lower the free energy.

Maier and Meier [2] showed that $\Delta\varepsilon$ can be written in the form

$$\Delta\varepsilon = A[\,\Delta\chi_e - Bp^2/T\,]\,S \tag{4.5}$$

where A is proportional to the number of molecules/cc and hence indirectly depends on temperature, $\Delta\chi_e$ is the polarisability anisotropy and p is the longitudinal component of the permanent dipole moment. The second term depends on temperature explicitly. The experiments and theoretical calculations considered in this chapter are carried out over about 10^0C, *i.e.*, the temperature variation is less than about 10% of the absolute temperature (K). Thus, to a good approximation, we can write

$$\Delta\varepsilon = \Delta\varepsilon_1 S \tag{4.5a}$$

---

† Note that, in SI units, absolute permittivity is denoted as ε and the relative permittivity (or dielectric constant) is denoted as ε_r. For the sake of convenience we omit the subscript 'r' and use ε for dielectric constant.

and consider $\Delta\varepsilon_1$ as constant, where $\Delta\varepsilon_1$ is the dielectric anisotropy for the fully aligned state (*i.e.*, $S = 1$). Using this in equation 4.4, we can write,

$$\varepsilon_{\parallel} = \bar{\varepsilon} + \frac{2}{3}\Delta\varepsilon_1 S \tag{4.6}$$

where $$\bar{\varepsilon} = (\varepsilon_{\parallel} + 2\varepsilon_{\perp})/3 \tag{4.7}$$

is the average dielectric constant. Using equation 4.6, equation 4.5 can be written as

$$F^{E} = -\frac{1}{2}\varepsilon_0 \bar{\varepsilon}\mathcal{E}^2 - \frac{1}{3}\varepsilon_0 \Delta\varepsilon_1 S\mathcal{E}^2 \tag{4.8}$$

Assuming that $\bar{\varepsilon}$ remains unchanged, the free energy is lowered if S takes a higher value in presence of the field *i.e.*, the external field results in an additional orienting potential and leads to an increase of the nematic order parameter [3].

When an electric field is applied to an *isotropic* liquid *i.e.*, at a temperature above the N-I transition point, it induces a weak orientational order (paranematic phase). When the applied field is *not* very strong, the value of S due to the induced order in the paranematic (N_P) phase is very small. Thus, from the equation 4.8, neglecting the induced S part, the field dependent free energy density for the paranematic phase can be written as,

$$F^{E}_{NP} = -\frac{1}{2}\varepsilon_0 \bar{\varepsilon}\mathcal{E}^2 \tag{4.8a}$$

For a paranematic liquid crystal with *polar* molecules, $\bar{\varepsilon}$ can be 10 or more.

If the field is strong, the induced order parameter increases, especially just above the nematic-isotropic transition temperature (T_{NI}). Also, the nematic-paranematic (N-N_P) transition temperature, increases with field. Since both the N and the field induced N_P phases have the same symmetry, there can be a first order N-N_P transition with a jump in S or a continuous evolution of N to N_P beyond a critical point. This is analogous to the liquid-gas transition or the N_1-N_d transition (described in chapter-2). Thus, when the field is increased, the first order nature of the N-N_P transition becomes weaker and finally results in a continuous change-over from a strongly oriented to a

weakly oriented phase beyond a critical field [4, 5] (see figure 4.1). Experimental studies on the effects of strong electric field are hampered by the inevitable Joule heating of the sample due to the ionic currents and dielectric heating due to the relaxation of molecular dipoles at a relatively low frequency. Recently, Durand and co-workers [4, 6] have quantitatively studied the critical point in the nematic-paranematic phase transition by using short pulses of electric fields separated by a long time interval to allow the system to remain in thermal equilibrium. More recently, Madhusudana *et al* have developed an alternative experimental technique in which the *local* temperature of the sample is monitored to take account of the heating effect [7, 8]. There have been a number of theoretical calculations on the detailed phase diagrams in the presence of a field in the framework of the Landau theory [9, 10, 11]. There are also some molecular models that discuss this phenomenon [12, 13, 14].

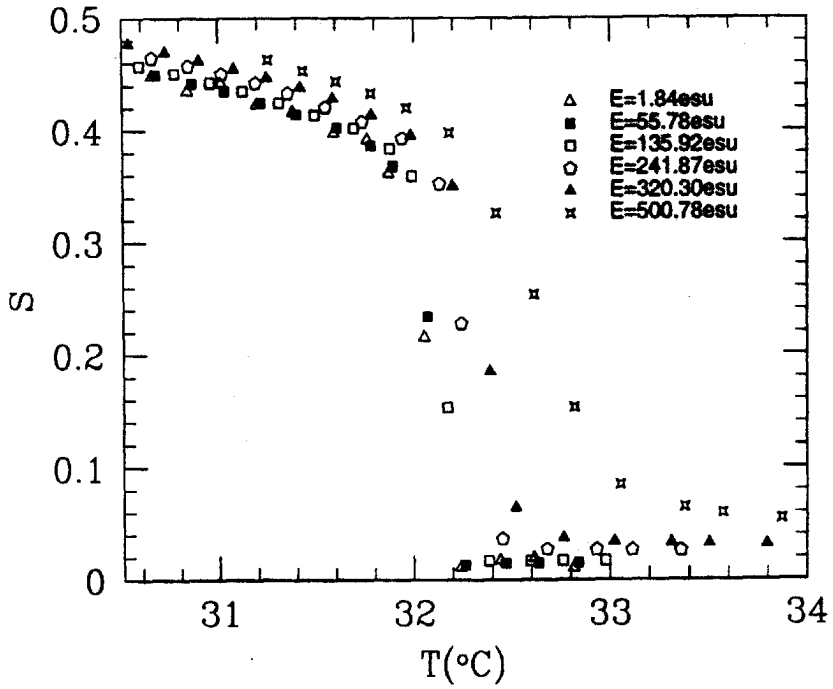

Figure - 4.1. Variation of the orientational order parameter (*S*) with respect to temperature, of the compound pentyl- cyanobiphenyl, under various external electric fields [5]. Note that the jump in *S* reduces to zero at higher fields and also *S* increases with field at any given temperature.

As described in the introduction, compounds which exhibit the N_R phase are highly polar. Hence, an external electric field can have a very strong influence on the orientational order of these compounds. This can in turn influence the N-SmA_d,

SmA_d-N_R and N_1-N_d phase transition temperatures. Experimental data [7] and the theories based on the Landau-de Gennes phenomenological model [7, 15] show that the smectic A-nematic transition temperature increases as the square of the applied field. Experiments also show that the temperatures of N_1-N_d transition, SmA_d-N_R transition and SmA_1-SmA_d transition, increase with the field [8, 16].

The strongly polar compound *p*-cyanophenyl *p-n* heptylbenzoate (CP7B) has a large positive $\Delta\varepsilon$ and ordinarily shows only a nematic phase. However, due to the enhancement of *S* under a strong external electric field [17] or in extremely thin cells [16], the compound shows a jump in *S* as the temperature is varied, indicating an N_1-N_d transition (see figure 4.2).

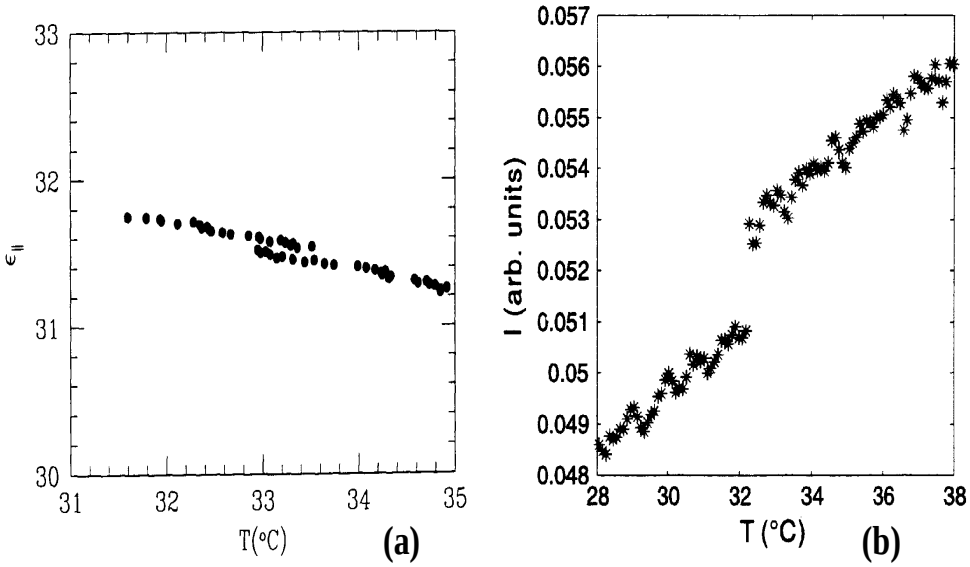

Figure - 4.2. (a) Variation of $\varepsilon_{\parallel}$ as a function of temperature for the compound CP7B in a cell of thickness of 10 μm under an alternating voltage of 180V and frequency 4111 Hz [17]. (b) Variation of transmitted intensity as a function of temperature for the compound CP7B for cell thickness of 1.9 μm. [16]. Note the jump in both the cases around 33^0 C indicating a jump in *S*.

Electric field phase diagrams have also been constructed [8] for the mixture of hexyloxy cyano-biphenyl (6OCB) and octyloxy cyanobiphenyl (8OCB) with 27wt % of 6OCB, which exhibits the N_R phase. The mixture has the following sequence of transitions in the absence of electric field:

Isotropic-(78.3^0C)-N-(47.2^0C)-SmA_d –(28.4^0C)-N_R.

The experimental electric field- temperature phase diagram is shown in figure 4.3. Both the SmA_d-N_R and SmA_d-N transition temperatures increase with field. The variation of the former is much stronger than that of the latter. Hence, for sufficiently high fields, the SmA_d phase can be expected to get bounded. This is reminiscent of the bounded SmA_d phase in pressure-temperature phase diagrams. However, due to practical difficulties, the applied voltages are limited to 300 V(at 4111 Hz). As the sample thickness is ~20μm, this is equivalent to 500 esu field. Though the field dependence of the SmA_d-N_R transition temperature is shown by a smooth line as a guide to the eye, note that the data indicates a change of slope at $\mathcal{E}\approx$200esu.

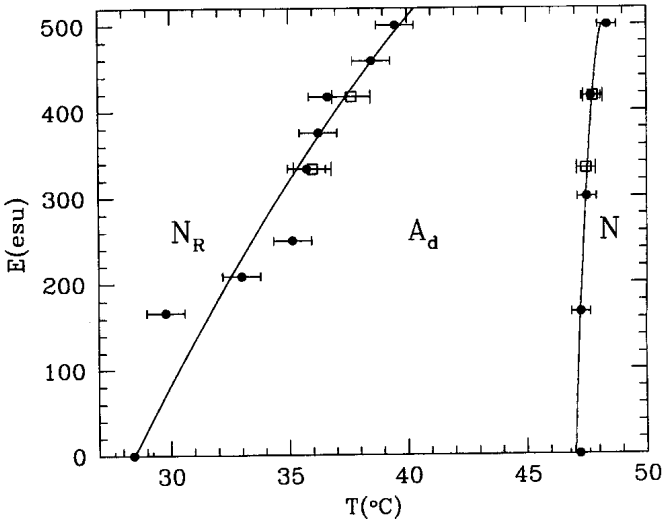

Figure - 4.3. The electric field-temperature phase diagram for a mixture of 27 wt % of 6OCB in 8OCB [8]. Circles and open squares are the data obtained from light scattering measurements and electrical impedance measurements respectively. The solid lines are guides to the eye. Note the slope change in the data points corresponding to SmA_d-N_R transition near a field of 200 esu.

In the next section we present a theoretical model to describe the electric field phase diagrams.

4.2 *Theoretical model*

4.2.1 Assumptions

We extend our molecular theory of highly polar compounds described in the previous chapters to include the effect of a strong electric field. Many of the

assumptions made in this model have already been discussed in the earlier chapters. We recall the assumptions relevant for the present theory.

(1) The medium is assumed to consist of 'pairs' of molecules having either antiparallel (A) or parallel (P) configurations. The difference between the pairing energy of the A-type (E_A) and the P-type (E_P) configurations is written as

$$\Delta E = E_A - E_P = R_1 k_B T_{NI}\left(\frac{R_2}{T_R} - 1\right) \tag{4.9}$$

where R_1 is an interaction parameter and R_2 is the reduced temperature at which the density of the medium is such that ΔE becomes zero.

(2) The orientational potential for A-type of pairs (U_{AA}) and P-type of pairs (U_{PP}) are assumed to be different. We write, as in chapter-2,

$$U_{PP} = Y U_{AA} \tag{4.10}$$

and the mutual interaction potential

$$U_{AP} = U_{PA} = P\sqrt{U_{AA}\, U_{PP}} \tag{4.11}$$

where $P \neq 1$ indicates a deviation from the geometric mean (GM) approximation.

(3) The McMillan parameters [18] for A-type (α_A) and P-type (α_P) configurations can be written as

$$\alpha_A = 2\exp(-[\pi r_o/(r_o + 2c)]^2) \tag{4.12}$$

$$\alpha_P = 2\exp(-[\pi r_o/(r_o + c)]^2) \tag{4.13}$$

where r_o and c are the lengths of the aromatic and chain moieties of the molecule respectively. The mutual smectic interaction parameter

$$\alpha_{AP} = \alpha_{PA} = \alpha_E = Q\sqrt{\alpha_A\, \alpha_P} \tag{4.14}$$

where $Q \neq 1$ indicates a deviation from the geometric mean (GM) approximation.

(4) Following Kventsel *et al* [19], we decouple the translational and orientational parts in the McMillan's 'mixed' order parameter (σ) and write

$$\sigma = S\tau \tag{4.15}$$

where S and τ are the nematic and the smectic order parameters respectively.

The following are the additional assumptions made to incorporate the effect of an external electric field.

(5) The electric field enhances the density of the medium (electrostriction). The 'direct' effect arises from the pressure due to the field [20],

$$p_E = \frac{\varepsilon_0 \varepsilon_\parallel \mathcal{E}^2}{2} \tag{4.16}$$

and yields

$$\frac{\delta\rho}{\rho} = \frac{\kappa_T \varepsilon_0 \varepsilon_\parallel \mathcal{E}^2}{2} \tag{4.17}$$

where κ_T is the isothermal compressibility. For the highest fields that are applied, $\delta\rho/\rho \sim 10^{-5}$. However, as we mentioned, the anisotropy of dielectric constant couples to the field to enhance the order parameter of the medium. This results in another contribution to the electrostriction:

$$\delta\rho = \left[\frac{\partial\rho}{\partial S}\right]_T \delta S(\mathcal{E}) \tag{4.18}$$

with

$$\delta S(\mathcal{E}) \approx \frac{\chi \Delta\varepsilon_1 \mathcal{E}^2}{3} \tag{4.19}$$

where χ is the susceptibility for the orientational order[‡] and is assumed to be $\sim 4\times10^{-8}$ (cgs units) [6] in the present calculations. With $\Delta\varepsilon_1 \approx 15$ and $\mathcal{E} \approx 600$esu , equation 4.19 gives $\delta S \approx 6\times10^{-3}$. Horn [21] has measured the order parameter of pentyl cyanobiphenyl as a function of pressure and at temperatures much lower than T_{NI}, $[\partial\rho/\partial S]_T \approx 0.3$. Using these values in equation 4.18, since $\rho \approx 1$gm/cc, we have, $\delta\rho/\rho \approx 2 \times 10^{-3}$, which is 200 times larger than the direct electrostriction effect estimated earlier. Hence the intermolecular separation decreases considerably and this can in turn be expected to change R_2 .

In view of the above discussions, we can write:

$$R_2(\mathcal{E}) = R_2(0) + C\,\mathcal{E}^2. \tag{4.20}$$

The value of C is estimated as follows:

[‡] Note that $(1/\chi)$ has the unit of energy density. Therefore $\chi = 4\times10^{-8}$ cc/erg = 4×10^{-7} m^3/J. Also, 1esu = 3×10^4 V/m.

As ρ increases, the intermolecular separation r decreases and hence ΔE increases (see figure 2.5, chapter-2). From our earlier calculation (see section 2.2, chapter-2) of the variation of ΔE (given by equation 4.9) with r, for $r \approx 5$Å it is found that

$$\partial(\Delta E)/\partial r \approx 10^{-19} \text{ J/Å}. \tag{4.21}$$

We have, $\delta\rho/\rho = 3\delta r/r \approx 2\times10^{-3}$. Hence, $\delta r/r \approx 10^{-3}$ and for $r \approx 5$Å, we have $\delta r \approx 5\times10^{-3}$Å. With this, equation 4.21 yields $\delta(\Delta E) \approx 5\times10^{-22}\text{J} = 5\times10^{-15}$ erg. Using equation 4.20 in 4.9, the increase in ΔE with field at $T_R = R_2(0)$ is given by

$$\delta(\Delta E) = R_1 k_B T_{NI} C \mathcal{E}^2/T_R. \tag{4.22}$$

As in the previous chapter, using $R_1 = 15$, $T_R = R_2(0) = 0.8$, $T_{NI} = 500$ K and with $\mathcal{E} = 600$esu, we get $C \sim 10^{-8}$ cgs units.

We have not taken into account the possible volume-dependence of the orientational and layering potentials, the affect of which will be much smaller than the one discussed above.

(6) Though there is no *long range* polar order in the medium, the P-type of pairs have a polar *short range* order. For each molecule in a P-type of pair, the permanent dipole in the neighbouring molecule induces an *oppositely* oriented dipole and reduces the net dipole moment (see figure 2.4, chapter-2). With the polarisability $\chi_e \approx 50\text{Å}^3$ and the intermolecular separation $r \approx 5$Å, the magnitude of the induced dipole moment is nearly half of that of the permanent dipole moment. Thus, if the permanent dipole moment of each molecule is p, the net dipole moment of a P-type of pair is also p. In the presence of an external electric field ($\vec{\mathcal{E}}$), this contributes a term linear in $\vec{\mathcal{E}}$, to the orienting potential of P-type of pairs. Also, due to the anisotropy in the polarisability of the aromatic cores, *both* A and P types of pairs have an orienting potential proportional to $\mathcal{E}^2$. Thus, in the presence of an external electric field, the additional orienting potentials of the i^{th} A-type and j^{th} P-type of pairs can be written as

$$U_{Ai}^{E}(\mathcal{E}) = -\gamma \mathcal{E}^2 \cos^2\theta_{Ai}$$

and

$$U_{Pj}^{E}(\mathcal{E}) = -p\,\mathcal{E}\cos\theta_{Pj} - \gamma \mathcal{E}^2 \cos^2\theta_{Pj} \tag{4.23}$$

The value of the coefficient γ is estimated as follows.

Including the orienting potential due to the field in the Maier-Saupe theory (reviewed in section 2.3, chapter-2), the single particle potential of the i^{th} molecule is given by

$$U_i = -U_0 S P_2(\cos\theta_i) - \gamma \mathcal{E}^2 \cos^2\theta_i \quad (4.24)$$

where γ is a constant assumed to be independent of S and $\mathcal{E}$. Hence, the value of γ is the same in the nematic and paranematic phases. Considering the paranematic (N_P) phase with $S \approx 0$, equation 4.24 can be written as,

$$U_i^{NP} = -\gamma \mathcal{E}^2 \cos^2\theta_i \quad (4.25)$$

Proceeding as usual, with the free energy $F = U - T\mathcal{S}$, we get

$$\frac{F^{NP}}{Nk_BT} = -\ln Z^{NP} \quad (4.25a)$$

where Z^{NP} is the normalising integral of the distribution function in presence of electric field. We have

$$Z^{NP} = \int_0^1 d(\cos\theta) \exp\left(\frac{\gamma \mathcal{E}^2}{k_BT} \cos^2\theta\right). \quad (4.25b)$$

Since $\gamma \mathcal{E}^2 << k_BT$, expanding $\ln Z^{NP}$ and collecting the leading term, we get, the free energy *per mole* with $\mathcal{E}$ in esu,

$$F^{NP} = -N\gamma \mathcal{E}^2/3. \text{(erg/mol)} \quad (4.26)$$

We compare this with the free energy *per unit volume* given in equation 4.8a for the paranematic phase. Since the experimental diagrams are usually plotted with the field in esu, we have carried out our calculations in esu to facilitate a direct comparison with the experimental data. Using the typical values of $\bar{\varepsilon}$ (≈15), density (≈ 1gm/cc) and molecular weight (≈ 300 gm/mol), from equations 4.26 and 4.8a we get $N\gamma \approx 540$ per mole.

In the MS theory, expressing $\cos^2\theta_i$ in equation 4.24 in terms of $P_2(\cos\theta_i)$, and proceeding as in section 2.3 (chapter-2), the final expression for the free energy per mole is

$$\frac{F}{Nk_BT} = + \frac{U_0}{2k_BT} S^2 - \frac{\gamma \mathcal{E}^2}{3k_BT} - \ln Z \tag{4.27}$$

where Z is the normalising integral, given by

$$Z = \int_0^1 \mathrm{d}(\cos\theta) \exp\left[\left(\frac{U_0}{2k_BT} S + \frac{2\gamma \mathcal{E}^2}{3k_BT}\right) P_2(\cos\theta)\right]. \tag{4.28}$$

The necessary integrals are solved numerically with $N\gamma$=540. For a given external field, the calculated free energies for the low S and high S solutions become equal at the N-N_p transition temperature ($T_{N\text{-}NP}$). For a field of 1000 esu, we get $T_{N\text{-}NP}$ about 4.5K higher than T_{NI} in the field free case, *i.e.*, an increase of 4.5×10^{-6} K/(esu)^2. This agrees quite well with the experimental [4, 22] value of 5×10^{-6}K/(esu)^2 for compounds with a cyano end group. Hence, we use, for a mole of *pairs*, $N\gamma$ = 1080.

4.2.2 Free energy and order parameters

As in the previous chapter (see section 3.4.1), extending the McMillan theory for mixtures, the potential energy of the i^{th} A-type of pair in the absence of electric field can be written as

$$\begin{aligned} U_{Ai} = & - U_{AA} X_A S_A P_2(\cos\theta_{Ai})[1 + \alpha_A \tau_A \cos(2\pi z_{i\,A}/d)] \\ & - U_{AP} X_P S_P P_2(\cos\theta_{Ai})[1 + \alpha_{AP} \tau_P \cos(2\pi z_{i\,A}/d)] \end{aligned} \tag{4.29}$$

where X_A, X_P, S_A, S_P and τ_A , τ_P are the mole fractions, orientational and translational order parameters of A and P types of pairs respectively. Similarly for a P-type pair, U_{pj} is obtained by interchanging suffixes A and P in equation 4.29. Experimentally, dc electric field is not used to avoid problems due to ionic conductivity. We assume that the frequency of ac is sufficiently low, so that the dipoles *follow* the field and we confine our calculations to a dc field. In presence of electric field, the dipoles have a long range polar order with an average orientation $\langle\cos\theta\rangle$. Thus, using equation 4.23, the internal energy of one mole of pairs in the presence of electric field can be written as

$$\begin{aligned} 2U = & \frac{NX_A}{2}\langle U_{Ai}\rangle + \frac{NX_P}{2}\langle U_{Pj}\rangle - NX_P \Delta E \\ & - N\gamma \mathcal{E}^2 (X_A \langle\cos^2\theta_{Ai}\rangle + X_P \langle\cos^2\theta_{Pj}\rangle) - Np\,\mathcal{E}\langle\cos\theta_{Pj}\rangle \end{aligned} \tag{4.30}$$

where the factor 2 on the left hand side reminds that we have a mole of pairs, the factor ½ appears in the first two terms since each pair is counted twice while averaging over the *mutual* interactions and we have also added the concentration dependent part of the configurational energy. Proceeding as in chapter-3, the molar entropy is given by:

$$2\mathcal{S} = -N k_B \left[X_A \frac{1}{d} \int_{-d/2}^{+d/2} dz_{Ai} \int_0^1 d(\cos\theta_{Ai})\, f_{Ai} \ln f_{Ai} + X_P \frac{1}{d} \int_{-d/2}^{+d/2} dz_{Pj} \int_0^1 d(\cos\theta_{Pj})\, f_{Pj} \ln f_{Pj} \right]$$

$$- N k_B (X_A \ln X_A + X_P \ln X_P) \tag{4.31}$$

where the last term is the entropy of mixing and f_A and f_P are the normalised distribution functions of A and P types of pairs respectively. The Helmholtz free energy is given by:

$$F = U - T\mathcal{S} \tag{4.32}$$

The distribution functions f_A and f_P are found by minimising F. It can be shown that the decoupling assumption [19] (see equation 4.15) leads to the result

$$f_A = f_{Ao}\, f_{At} \text{ , and } f_P = f_{Po}\, f_{Pt} \tag{4.33}$$

where f_{Ao} and f_{At} are the orientational and translational distribution functions of the A-type of pairs and f_{Po} and f_{Pt} are those for the P-type of pairs. We have

$$f_{Ao} = \frac{1}{Z_{Ao}} \exp\left\{ \left(\frac{U_{AA}}{k_B T} [\, X_A S_A (1+\alpha_A \tau_A^2) + P\sqrt{Y}\, X_P S_P (1+\alpha_E \tau_A \tau_P)] + \frac{2\gamma \mathcal{E}^2}{3 k_B T} \right) P_2(\cos\theta_A) \right\}$$

$$f_{Po} = \frac{1}{Z_{Po}} \exp\left\{ \left(\frac{U_{AA}}{k_B T} [\, Y X_P S_P (1+\alpha_P \tau_P^2) + P\sqrt{Y}\, X_A S_A (1+\alpha_E \tau_A \tau_P)] + \frac{2\gamma \mathcal{E}^2}{3 k_B T} \right) P_2(\cos\theta_P) + \frac{p\mathcal{E}}{k_B T} \cos\theta_P \right\}$$

$$f_{At} = \frac{1}{Z_{At}} \exp\left\{ \frac{U_{AA}}{k_B T} S_A [\alpha_A X_A S_A \tau_A + P\sqrt{Y}\, \alpha_E X_P S_P \tau_P] \cos(2\pi z_A / d) \right\}$$

$$f_{Pt} = \frac{1}{Z_{Pt}} \exp\left\{ \frac{U_{AA}}{k_B T} S_P [Y\alpha_P X_P S_P \tau_P + P\sqrt{Y}\alpha_E X_A S_A \tau_A] \cos(2\pi z_P / d) \right\} \tag{4.34}$$

where Z_{Ao}, Z_{Po}, Z_{At} and Z_{Pt} are the appropriate normalising integrals. Hence the order parameters are given by:

$$S_A = \int_0^1 d(\cos\theta_{Ai}) P_2(\cos\theta_{Ai})\, f_{Ao} \tag{4.35}$$

and

$$\tau_A = \int_0^1 d(\zeta_A)\cos(\pi\zeta_A)\, f_{At} \tag{4.36}$$

where the reduced co-ordinate $\zeta_A = (2z_A/d)$ is used. S_P and τ_P are obtained by interchanging the suffixes A and P in equations 4.35 and 4.36. The free energy per mole of pairs can now be written in the simplified form

$$2F = +\frac{N U_{AA}}{2}[X_A^2 S_A^2(1+3\alpha_A \tau_A^2) + Y X_P^2 S_P^2 (1+3\alpha_P \tau_P^2) + 2P\sqrt{Y} X_A X_P S_A S_P(1+3\alpha_E \tau_A \tau_P)]$$

$$-\frac{1}{3} N \gamma \mathcal{E}^2 - Nk_BTX_A \ln\left(\frac{Z_{Ao} Z_{At}}{X_A}\right) - Nk_BTX_P \ln\left(\frac{Z_{Po} Z_{Pt}}{X_P}\right) - NX_P \Delta E \tag{4.37}$$

The terms depending on S and $\langle\cos\theta\rangle$ cancel in F on substituting equations 4.34 in equation 4.31 for entropy. However, the '$p\mathcal{E}$' part affects S_P and hence F through f_{PO} (see equation 4.34). The equilibrium value of the mole fraction of the A-type of pairs (X_A)is found by minimising F with respect to X_A. We get, with $X_P = 1 - X_A$,

$$\frac{X_P}{X_A} = \frac{Z_{Po} Z_{Pt}}{Z_{Ao} Z_{At}} \exp\left\{\frac{U_{AA}}{k_BT}[\alpha_A X_A S_A^2 \tau_A^2 - Y\alpha_P X_P S_P^2 \tau_P^2 + P\sqrt{Y}\,\alpha_E S_A S_P \tau_A \tau_P (X_P - X_A)] + \frac{\Delta E}{k_BT}\right\} \tag{4.38}$$

Calculations have been made as in the previous chapters, for $R_2(0) = 0.8$ and 0.6 with $R_1 = 15$ and 6. We have used p= 4D and $N\gamma$ =1080. Thus, at low fields, $Np\mathcal{E}$ (~$10^6\,\mathcal{E}$) is much larger than $N\gamma\mathcal{E}^2$ (~$10^3\,\mathcal{E}^2$), and we can expect the polar short range order to have significant effect at low fields, especially when X_P is relatively large. We evaluate all the necessary integrals using a 32 point Gaussian quadrature method in double precision. We look for the following types of solutions:

1) S_A, $S_P \neq 0$, $\tau_A = \tau_P = 0$ leading to nematic phase which is N_1 if X_A is relatively small and N_d if X_A is relatively large, and,

2) S_A, $S_P \neq 0$, τ_A , $\tau_P \neq 0$ leading to the smectic phase which is SmA_1 if X_A is relatively small and SmA_d if X_A is relatively large.

The average orientational order parameter is given by

$$\bar{S} = X_A S_A + X_P S_P \tag{4.39}$$

4.2.3 Results and discussion

4.2.3.1 Effect of electric field on the nematic - paranematic transition

We first consider the simplest case in which $P = Q = 1$, *i.e.*, the geometric mean rule is assumed to be valid and further $Y = 1$, *i.e.*, the orientational potentials for both A and P types of pairs are equal. When the field is applied, the first order N-I transition changes over to first order nematic(N)-paranematic(N_P) transition. The first order transition ends in a critical point as the field is increased. This behaviour is seen in the variation of the average orientational order parameter shown in figure 4.4 for $R_1 = 15$, $R_2(0) = 0.8$. The transition is associated with a negligible jump in X_A. The theoretical variation compares qualitatively with the experimental diagram shown in figure 4.1. However, experimentally the critical temperature of the N-N_P transition is ~1K above T_{NI} (=300K) whereas the calculated critical temperature is about 15K above T_{NI} (see figure 4.4). Also, the calculated critical field is about 3 times larger than the experimental value. The mean field theory is known to overestimate the values of the critical temperature and field [14].

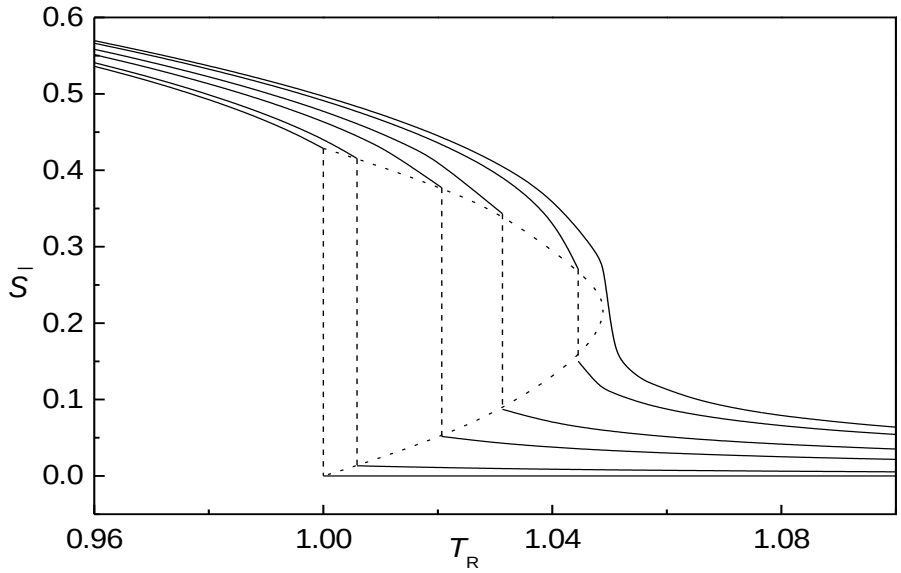

Figure - 4.4. Variation of the average orientational order parameter $\bar{S}$ at the first order nematic-paranematic transition, with R_1 = 15, R_2 = 0.8, and $P = Q = Y$ =1. The lines from left to right correspond to an external electric field $\mathcal{E}$= 0, 500, 1000, 1250, 1500 and 1650 esu respectively.

The N-N_P transition temperature increases quadratically with the external field. With T_{NI} = 500K and with the same set of parameter values used for figure 4.4, the calculated variation of $\Delta T = T_{N\text{-}NP} - T_{NI}$ in kelvin, as a function of $\mathcal{E}^2$ is shown in figure 4.5a. It can be seen that the slope $\Delta T/\mathcal{E}^2 \approx 10^{-5}$ K/(esu)^2 agrees with the experimental value ($\approx 5\times10^{-6}$ K/(esu)^2 [22]), for a compound with a cyano end group (having $T_{NI} \approx$400K). The calculated increase in the order parameter $\Delta S = S(\mathcal{E}) - S(0)$ as a function of $\mathcal{E}^2$ is shown in figure 4.5b. At T_R = 0.96 (figure 4.5b, line i), ΔS varies quadratically with the external field and the slope $\Delta S/\mathcal{E}^2 \approx 10^{-8}$/(esu)^2. At low values of T, S is relatively high and the susceptibility χ (*i.e.*, $\chi \sim \Delta S/\mathcal{E}^2$, see equation 4.19) is low and nearly constant with respect to electric field. At higher values of T (T_R = 1), S is low and χ is high. Also, as the electric field is increased, S increases significantly and hence χ decreases. Since χ varies with $\mathcal{E}$, ΔS is no longer quadratic in $\mathcal{E}$ and tends to have slower variation with field for higher fields (figure 4.5b, line ii). The average slope increases to 3.5×10^{-8}/(esu)^2 at T_R =1.0.

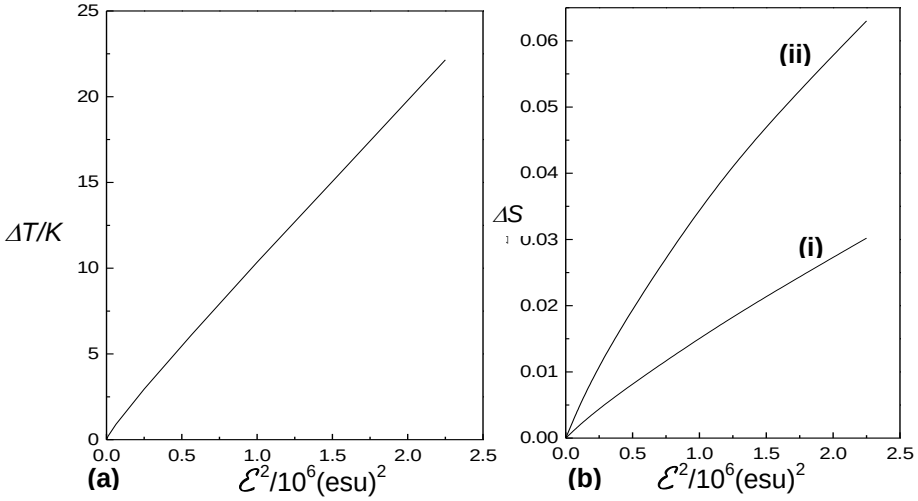

Figure - 4.5. Variation of (a) $\Delta T = T_{N\text{-}NP} - T_{NI}$ in kelvin and (b) increase in the order parameter $\Delta S = S(\mathcal{E}) - S(0)$ for (i) $T_R = 0.96$and (ii) $T_R = 1.0$, as functions of $\mathcal{E}^2$, for the set of parameters as in the figure 4.4.

The calculated quadratic enhancement of S due to the field is microscopic in origin and is usually known as the Kerr effect. From the experimental data [17] for the compound CP7B, extracting the contribution from the Kerr effet only, it is shown that [17] $\chi \sim 10^{-7}$/(esu)^2 and increases with temperature.

4.2.3.2 Effect of electric field on the N_1-N_d transition

As already described in chapter-2 (see section 2.4.3), we get a first order N_1-N_d transition for $R_1 = 15$, $R_2(0) = 0.8$, $P = 0.71$ and $Y = 2$. We have calculated the effect of an external electric field on the N_1-N_d transition using these parameters. The temperature variations of X_A and the average order parameter $\bar{S}$ associated with the transition are shown in figure 4.6(a) and (b) respectively. We see that, as the field is increased, the first order N_1-N_d transition ends in a critical point at $\mathcal{E} \approx 1100$esu and at $T_R \approx 0.9$. The calculated increase in the N_1-N_d transition temperature (ΔT) is plotted with respect to $\mathcal{E}^2$ in figure 4.7.

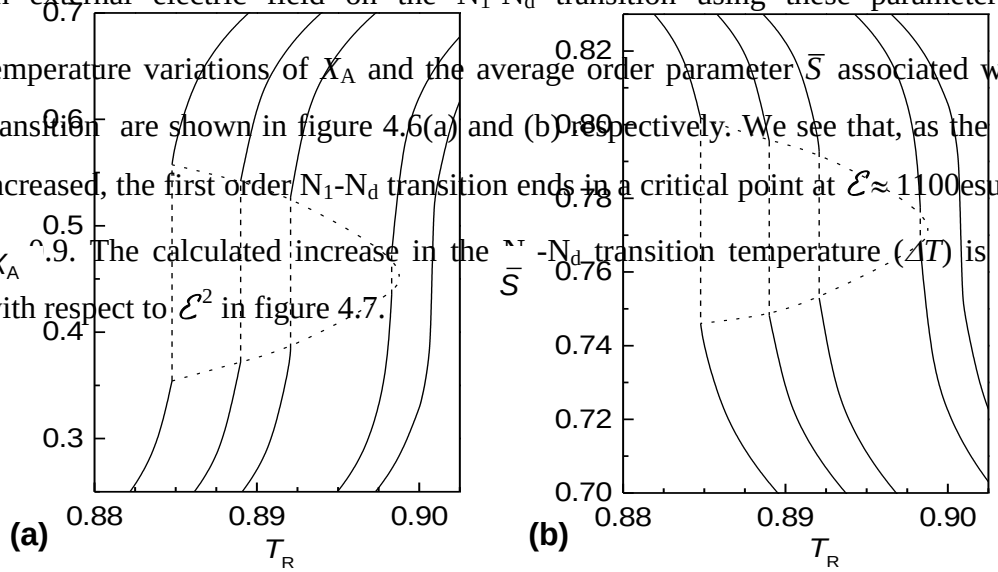

Figure - 4.6. Variation of (a) the mole fraction of the A type of pairs (X_A) and (b) the average order parameter ($\bar{S}$) as functions of the reduced temperature with R_1 = 15, R_2 = 0.8, P =0.71 and Y = 2. The lines from left to right correspond to the external field $\mathcal{E}$=0, 500, 700, 1000 and 1100 esu respectively.

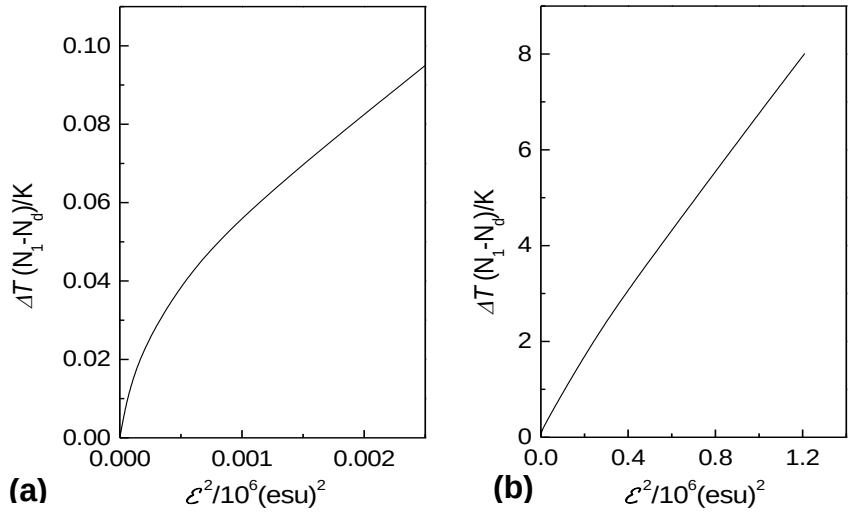

Figure - 4.7. (a)Variation of the shift in the N_1-N_d transition temperature at low fields, as a function of $\mathcal{E}^2$ with T_{NI} = 500K, for the parameter set as in figure 4.6. The slope is constant at high fields (b).

As mentioned earlier (see section 4.22), the linear term dominates at low fields and ΔT is large (figure 4.7a). For example, at $\mathcal{E}$ = 10 esu, slope $\Delta T/\mathcal{E}^2 \approx 2\times10^{-4}$ K/(esu)^2. As the external field is increased, the $\mathcal{E}^2$ term dominates and the slope decreases. A graph of ΔT vs $\mathcal{E}^2$ at high fields is practically a straight line (figure 4.7b), with the slope $\approx 7\times10^{-6}$ K/(esu)^2. It is clear that the enhancement of ΔT at low fields is due to the presence of *polar* short range order in the medium. Experimentally [16], for the compound CP7B contained in a thin cell, it is estimated that a field of 300V/mm (=10 esu) increases the N_1-N_d transition temperature by about 1^0C, which corresponds to $\Delta T/\mathcal{E}^2 \approx 10^{-2}$K/(esu)^2. The experimental value of ΔT is nearly 50 times the calculated value ($\approx$ 0.02K for 10 esu). This may be due to the presence of clusters with more than two molecules in the P-type configuration, thus enhancing the *polar* short range order effect. On the other hand, for the N-N_P transition, as mentioned earlier, X_A is relatively large and has a negligible jump at the transition. Hence, the linear coupling with field does not have a significant influence.

4.2.3.3 Effect of electric field on the reentrant transitions

As described in chapter-3 (see section 3.4.2), with $P = Q = Y = 1$ and $R_1 = 15$, $R_2(0) = 0.8$ and $\alpha_A = 1.05$, a double re-entrant sequence, *viz*, N-SmA_d-N_R-SmA_1, can be obtained as the temperature is lowered. With the same set of parameters and with $C = 10^{-8}$ cgs units as estimated after equation 4.20, we have calculated the effect of electric field on the N-SmA_d and SmA_d-N_R transition temperatures. The results are shown in figure 4.8a. The SmA_d range with $\mathcal{E} = 0$ is relatively large (~90^0C) compared to that of the experimental system (see figure 4.3). At low fields, as in the experimental system, both the N-SmA_d and SmA_d-N_R transition temperatures increase with field. The lower transition temperature increases more rapidly than the upper one. As the field is increased beyond some value, the N-SmA_d transition temperature actually starts to *decrease*. This would imply that for a large enough field, the SmA_d phase can disappear. This is reminiscent of the bounded nature of SmA_d phase in pressure-temperature phase diagrams. Indeed if we reduce R_1 to 6 and α_A to 0.96, we get the phase diagram with bounded SmA_d region (figure 4.7b) for $\mathcal{E} \approx 400$esu. In this case, when $\mathcal{E} = 0$, as in the experimental system, the SmA_d range is $\approx 0.05 T_{NI} \approx 18^0$C, using $T_{NI} \approx 350$ K (see section 4.2). The N-SmA_d transition temperature decreases with field even at low fields.

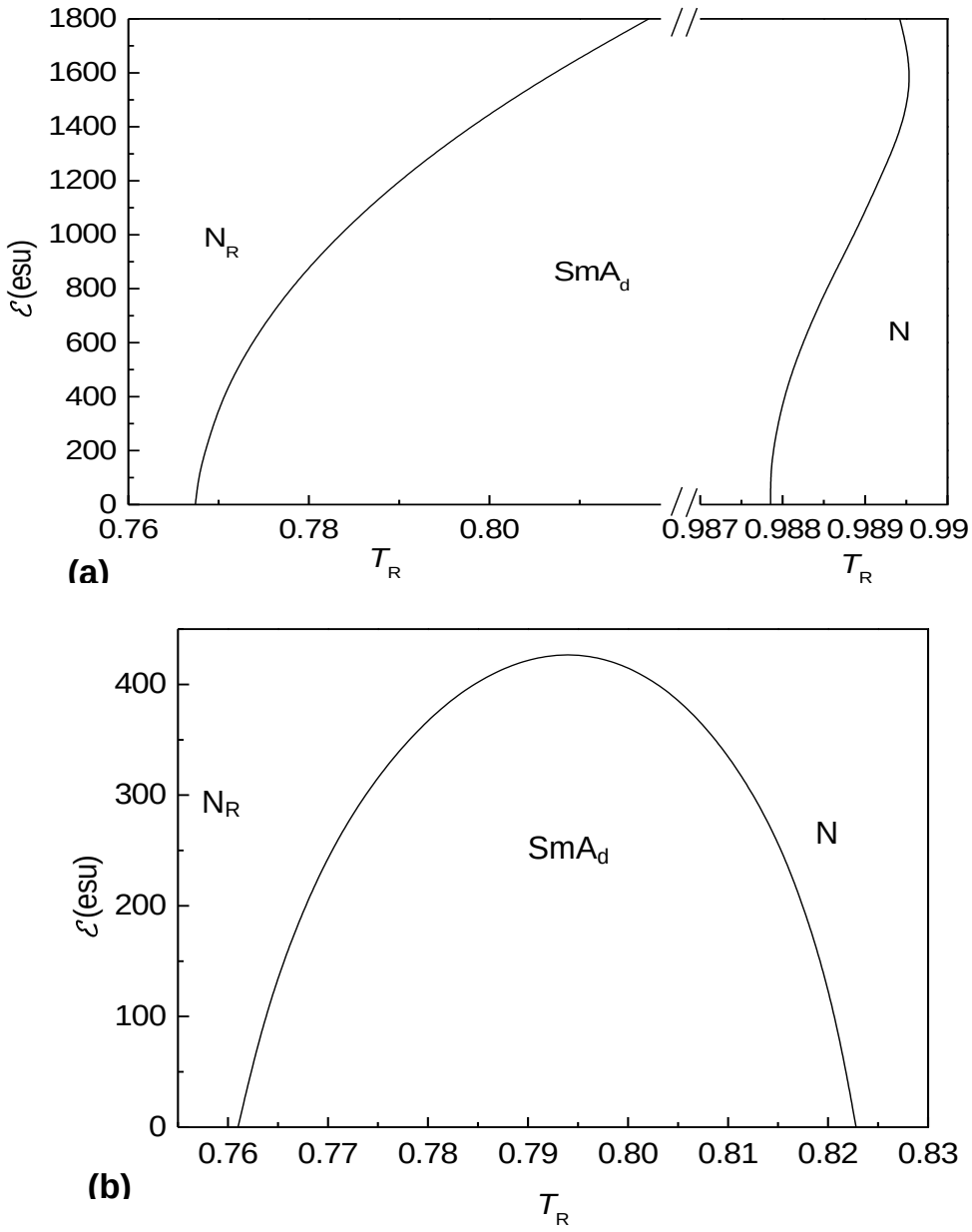

Figure- 4.8. (a) Calculated phase diagram showing N_R-SmA_d and SmA_d-N transition temperatures as functions of electric field $\mathcal{E}$ with $P = Q = Y = 1$, $R_1 = 15$, $R_2(0) = 0.8$, $\alpha_A = 1.05$ and $C = 10^{-8}$ cgs units. Note that the temperature scales are different for the two transitions. (b) Calculated phase diagram showing bounded SmA_d region obtained when R_1 and α_A are reduced to 6 to 0.96 respectively.

We have also calculated the electric field phase diagram which exhibits an N_1-N_d transition line in addition to the reentrant phases. For this, we use the set of parameters *viz*, $R_1 = 15$, $R_2(0) = 0.6$, $P = 0.7935$, $Y = 2$, $Q = 1$ which gives an N_1-N_d transition associated with double reentrance for $\alpha_A < 0.542$, as shown in chapter-3 (see text in section 3.4.2.2 and figure 3.21).

With $\mathcal{E}$=0, for α_A = 0.56, there is no N_1-N_d transition and the SmA_d range is 18^0C in this case also. With $\mathcal{E} \neq 0$, for α_A = 0.56, the N_1-N_d transition appears at higher fields. The electric field –temperature phase diagram obtained with $C = 10^{-8}$ cgs units is shown in figure 4.9. At $\mathcal{E} \sim 300$ esu, the SmA_d-N_R branch bifurcates showing a nematic-nematic transition. As in the previous chapters, we have indicated the two nematic liquid crystals which arise in the reentrant region by N_1 and N_d, which signify that N_1 has a higher concentration of P-type of pairs compared to the N_d phase. Above 400 esu, the SmA_d-N_R line varies more rapidly with field than at lower fields and the SmA_d phase is bounded.

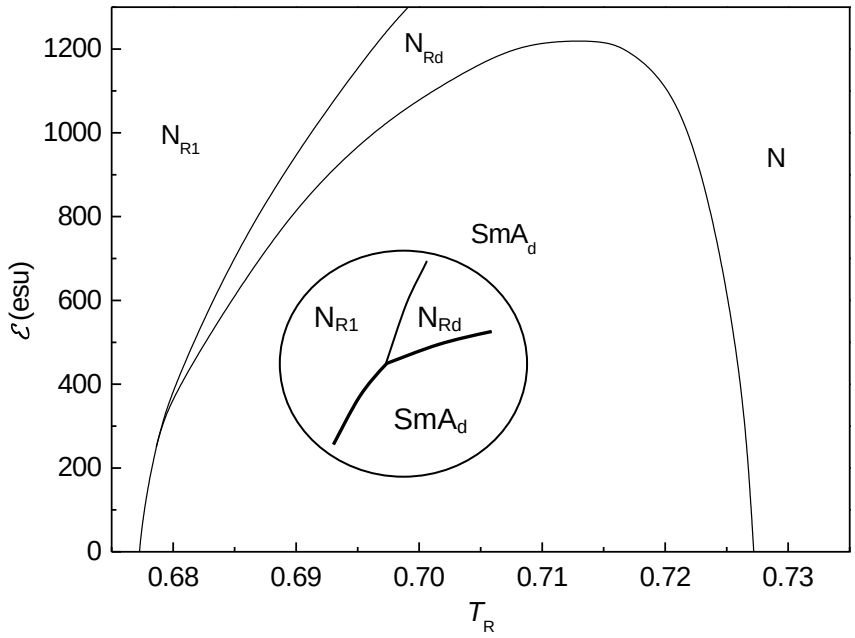

Figure - 4.9. Calculated phase diagram showing the nematic-nematic transition line branching off from N_R-SmA_d transition line at $\mathcal{E} \approx 300$ esu and $T_R \approx 0.679$, for R_1 = 15, $R_2(0)$= 0.6, P = 0.7935, Y = 2 , Q = 1, α_A = 0.56 and $C = 10^{-8}$ cgs units . The inset shows the topology near the branching point on an exaggerated scale.

As we have discussed in chapter-2 (see section 2.4.3), as a function of either P or Y, the first order N_1-N_d transition ends in a critical point at which X_A varies continuously. In the present calculations, the N_1-N_d transition ends in a critical point as a function of field as already described in section 4.2.3.2. For the present set of parameters, the jump in X_A decreases as the field is increased and we have not extended our calculations all the way to the critical point. In the experimental phase diagram (figure 4.3), the change in the slope of the SmA_d-N_R line is opposite to the

one shown in figure 4.9 (the thick line in the inset). As such, it is unlikely that the possible change of slope is associated with the development of N_1-N_d transition.

In all the above calculations, the value of C in equation 4.20 was taken to be 10^{-8} cgs units on the basis of experimental data on 5CB. The dielectric measurements on the 6OCB-8OCB mixture used in the experiment [8] clearly indicate that the susceptibility χ has a value $\approx 3 \times 10^{-7}$ near the N_R -SmA transition temperature. The larger value shows that the concentration of parallel pairs is relatively high in this mixture, compared to that in 5CB, as it should be for the occurrence of the reentrant nematic phase. This value of χ is about 8 times the earlier value used to estimate C (see discussion under assumption -5, section 4.2.1). Hence, in the next calculations we assume that $C = 8 \times 10^{-8}$ cgs units in equation 4.20. We have made calculation on the influence of the electric field on the phase diagram for the following set of parameters, $R_1 = 15$, $R_2(0) = 0.6$, $Q = 0.55$, $\alpha_A = 0.95$ and $P = Y = 1$, which gives a SmA_1-SmA_d transition associated with double reentrance, as shown in chapter-3 (see section 3.4.2.2).The phase diagram obtained is shown in figure 4.10.

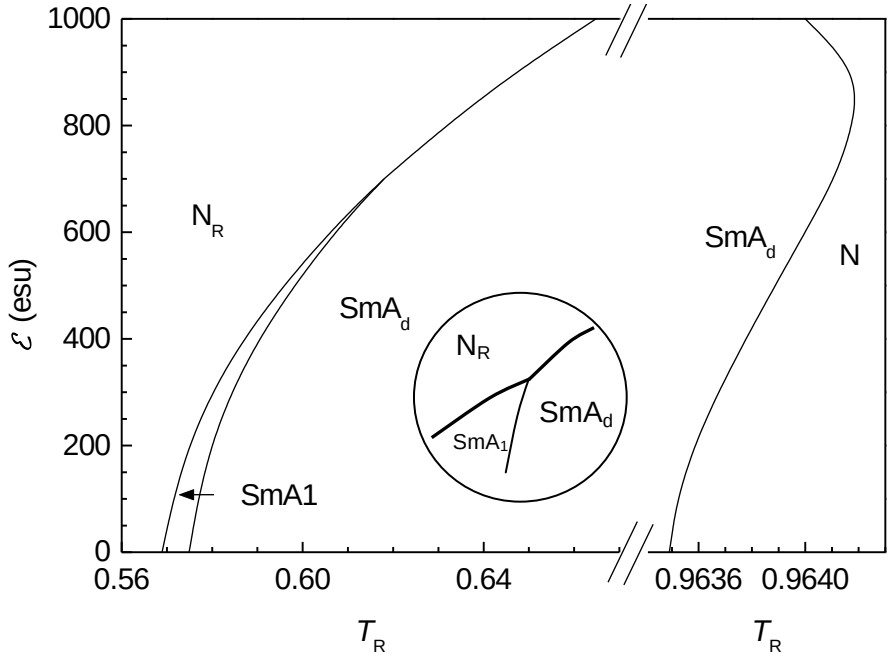

Figure - 4.10. Calculated phase diagram showing the SmA_1-SmA_d transition line meeting the N_R-SmA_d transition line at $\mathcal{E} \approx 700$ esu and at $T_R \approx 0.618$ for $R_1 = 15$, $R_2(0) = 0.6$, $Q = 0.55$, $\alpha_A = 0.97$, $P = Y = 1$ and $C = 8 \times 10^{-8}$ cgs units. Note that the temperature scale for the SmA_d-N transition is different from that for the N_R-SmA_d transition. The inset shows the topology near the meeting point on an exaggerated scale.

Both the SmA_d-SmA_1 and SmA_1-N_R transition temperatures increase with field. However, the SmA_1 range decreases and finally the SmA_d-SmA_1 and SmA_1-N_R transition lines meet at $\mathcal{E} \approx 700$ esu. At higher fields, only an SmA_d-N_R transition is realised. The change of slope of the smectic to N_R transition line (thick line in the inset of figure 4.10) is now similar to that seen in the experimental diagram (see figure 4.3). X-ray studies have been conducted by Cladis [23] on the mixture used in generating the experimental diagram shown in figure 4.3. However, X-ray measurement is not accurate enough to have detected a smectic A to smectic A transition. It would be interesting to look for such a transition in the system investigated. We should however note that in view of the approximations made in developing the molecular model and in particular with the mean field approach, quantitative agreement between the theoretical calculations and experimental data cannot be expected.

4.3 Conclusions

In this chapter, we have included the effect of an electric field in our molecular model of reentrant phases in highly polar compounds, in which the mutual orientation of near neighbour molecules changes from an antiparallel (A) to a parallel (P) configuration as the temperature is lowered. It is argued that the A to P cross-over temperature increases with field which accounts for the observed trends. By using a combination of linear and quadratic couplings of the orienting potential with field, we have shown that, as the field is increased, the first order nematic-paranematic as well as the N_1-N_d transition temperatures increase and the SmA_d phase gets bounded. Comparison of the results with the available experimental data shows that the linear coupling with field for P-type of pairs does not have significant influence on the nematic-paranematic transition since the concentration of the P-type of pairs (X_P) is small near the transition. On the other hand, X_P is quite high near the N_1-N_d transition. Thus, the linear term has significant influence on the N_1-N_d transition. This results in a large increase of the N_1-N_d transition temperature, especially at low fields. For suitable values of parameters, we have shown that either a nematic-nematic transition line can branch off from the SmA_d-N_R line or a SmA_1-SmA_d transition line can meet the SmA_d-N_R line at an appropriate field. In the latter case, the smectic to N_R

transition line has an associated slope change which is consistent with the available experimental data.

4.4 References for chapter-4

[1]de Gennes, P.G. and Prost, J., *The Physics of Liquid Crystals*, second edition (Clarendon, Oxford, 1993).

[2] Maier, W., and Meier, G., *Z. Naturforsch*, **16a**, 262, 1961, *ibid*, p.470.

[3] Dunmur, D. A., and Palffy-Muhoray, P., *J. Phys. Chem*., **92**, 1406, 1988.

[4]Lelidis I., Nobili, M. and Durand G., *Phys.Rev. E*, **48**, 3818, 1993.

[5]Geetha Basappa, Thesis, chapter-3, *Raman Research Institute, Bangalore*.

[6]Lelidis, I., and Durand, G., *Phys. Rev. E*, **48**, 3822, 1993.

[7] Geetha Basappa and Madhusudana, N.V., *Mol.Cryst.Liq.Cryst.*, **288**, 161, 1996.

[8] Geetha Basappa, Govind, A. S., and Madhusudana, N. V., *J. Phys. II France*., **7**, 1693, 1997.

[9] Fan, C., and Stephen, M. J., *Phys. Rev. Lett*, **25,** 500, 1970.

[10] Hornreich, R. M., *Phys. Lett*, **A109,** 232, 1985.

[11] Gramsbergen, E. F., Longa, L, and de Jeu, W.H., *Phys. Rep*, **135**, 195, 1986.

[12] Hanus, J., *Phys. Rev*, **178,** 420, 1969.

[13] Wojtowicz, P. J., and Sheng, P., *Phys. Lett*, **A48,** 235, 1974.

[14] Savithramma, K. L., and Madhusudana, N.V., *Mol.Cryst.Liq.Cryst.*, **103**, 99, 1983.

[15]Lelidis, I., and Durand, G., *J. Phys II*, **6**, 1359, 1996.

[16]Sobha, R. Warrier, Vijayaraghavan, D., and Madhusudana, N.V., *Europhysics Lett*, **44**(3), 296,1998.

[17] Geetha Basappa and Madhusudana, N.V., *Eur. Phys. J. B*, **1**, 179,1998.

[18]McMillan, W. L., *Phy. Rev. A*, **4**, 1238, 1971.

[19]Katriel, J. and Kventsel, G. F., *Phys.Rev.A*, **28**, 3037,1983.

[20]Tareev, B., *Physics of Dielectric Materials*, (Mir Publishers, Moscow, 1979), Chapter-2, p.135.

[21]Horn, R.G. and Faber, T.E., *Proc. R.Soc. Lond.A.*, **368,** 199, 1979.

[22]Helfrich, W., *Phys.Rev. Lett*, **24**, 201, 1971.

[23]Cladis P.E., *Mol.Cryst.Liq.Cryst*, **67**, 177, 1981.